Added value of multiangular measurements for estimating forest variables from the top of the atmosphere using coupled radiative transfer models

Laurent, Valérie C E ; Verhoef, W ; Clevers, J G P W ; Schaepman, Michael E

Abstract: Numerous studies have demonstrated the higher information content of multiangular reflectance data that can be used to improve the estimation of variables for surfaces having strong directional properties such as forests. Only a few studies, however, used physically- based radiative transfer (RT) models, and they were based on atmospherically-corrected data. The objective of this study was to investigate the potential of multi-angular top-of-atmosphere (TOA) radiance data for estimating surface variables using a coupled canopy-atmosphere model. The study area consisted of three Norway spruce stands located in the Czech Republic for which field data and a multi-angular set of four CHRIS/PROBA images were collected in September 2006. The coupled SLC (Soil-Leaf- Canopy) - MODTRAN model provided good simulations of the spectral and angular signatures measured by CHRIS. Local sensitivity analyses were performed to help with the model inversion. The singular values of the Jacobian matrix showed that the dimensionality of the estimation problem increased from 3 to 6 when increasing the number of angles from 1 to 4. One LUT was built for each stand, using the 7 most influential parameters: vertical crown cover, fraction of bark, tree shape factor, dissociation factor, and needle chlorophyll, dry matter, and brown pigments contents. All angular combinations were tested for estimating the variables. The best results were obtained when using two or three angles. The results show that although multi-angular TOA radiance data do have a higher potential than mono-angular data, it is still difficult to make full use of the information they contain for estimating forest variables.

ADDED VALUE OF MULTIANGULAR MEASUREMENTS FOR ESTIMATING FOREST VARIABLES FROM THE TOP OF THE ATMOSPHERE USING COUPLED RADIATIVE TRANSFER MODELS

V.C.E. Laurent [a, *], W. Verhoef [b], J.G.P.W. Clevers [a], M.E. Schaepman [c]

[a] Centre for Geo-Information, Wageningen University, P.O. Box 47, 6700 AA Wageningen, the Netherlands - (valerie.laurent, jan.clevers)@wur.nl

[b] Faculty of Geo-Information Science and Earth Observation (ITC), University of Twente, P.O. Box 6, 7500 AA Enschede, the Netherlands - verhoef@itc.nl

[c] Remote Sensing Laboratories, University of Zurich - Irchel, Winterthurerstr. 190, CH8057 Zurich, Switzerland - michael.schaepman@geo.uzh.ch

KEY WORDS: top-of-atmosphere, multi-angular, variable estimation, radiative transfer, forest, CHRIS/PROBA, SLC, MODTRAN.

ABSTRACT:

Numerous studies have demonstrated the higher information content of multiangular reflectance data that can be used to improve the estimation of variables for surfaces having strong directional properties such as forests. Only a few studies, however, used physically-based radiative transfer (RT) models, and they were based on atmospherically-corrected data. The objective of this study was to investigate the potential of multi-angular top-of-atmosphere (TOA) radiance data for estimating surface variables using a coupled canopy-atmosphere model. The study area consisted of three Norway spruce stands located in the Czech Republic for which field data and a multi-angular set of four CHRIS/PROBA images were collected in September 2006. The coupled SLC (Soil-Leaf-Canopy) - MODTRAN model provided good simulations of the spectral and angular signatures measured by CHRIS. Local sensitivity analyses were performed to help with the model inversion. The singular values of the Jacobian matrix showed that the dimensionality of the estimation problem increased from 3 to 6 when increasing the number of angles from 1 to 4. One LUT was built for each stand, using the 7 most influential parameters: vertical crown cover, fraction of bark, tree shape factor, dissociation factor, and needle chlorophyll, dry matter, and brown pigments contents. All angular combinations were tested for estimating the variables. The best results were obtained when using two or three angles. The results show that although multi-angular TOA radiance data do have a higher potential than mono-angular data, it is still difficult to make full use of the information they contain for estimating forest variables.

1. INTRODUCTION

Forests are important components of the Earth's surface because of their extensive area and their role in the carbon and climate cycles. Remote sensing is an efficient way to monitor them. Forest environments present anisotropic optical properties because of their internal structure, and multiangular data have been shown useful for obtaining more accurate estimates of bio-physical (Heiskanen, 2006; Rautiainen et al., 2008) and bio-chemical variables (Huber et al., 2010). Most multiangular estimation studies were based on atmospherically-corrected data, and only few of them made use of physical radiative transfer (RT) models (Schaepman et al., 2009). However, since the atmosphere also has anisotropic properties, it is important to understand the angular behaviour of the full canopy-atmosphere system (Pandya et al., 2007). Coupled canopy-atmosphere physical RT models directly relate the canopy and atmospheric variables to the radiance observed by the satellite at the top of the atmosphere (TOA). Such a coupled model can therefore be inverted directly using the TOA radiance data to obtain the surface variables. This approach is theoretically more accurate because the atmospheric effects are included in the forward model and it minimizes the data pre-processing as no atmospheric correction is needed (Laurent et al., 2011).

The objective of this study was to investigate the potential of multiangular TOA radiance data for estimating forest variables, by inverting a coupled canopy-atmosphere RT model.

2. MATERIALS AND METHODS

2.1 Study area and data

The study area consisted of three Norway spruce (*Picea abies* (L.) Karst.) stands, named YOUNG, OLD1 and OLD2, located at the Bily Kriz research site in Eastern Czech Republic (Table 1). The field data were collected in the first half of September 2006. The plant area index (PAI), defined as half of the total plant area, was averaged over the values obtained from LAI-2000, TRAC, and hemispherical photographs (Homolová et al., 2007). The woody-to-total correction factor used by Homolová et al. to obtain LAI from PAI was taken as the fraction of brown material in the PAI (fB). The crown length and diameter required to calculate the tree shape factor (Zeta) were measured using a laser rangefinder Impulse 200. The crown cover (Cv) was estimated by classifying an AISA image acquired on September 14th, 2006 (Lukeš, 2009). The spectral properties

* Corresponding author.

of the main background components and bark were measured using an ASD field spectrometer.

The CHRIS dataset was acquired on September 12th, 2006, in chlorophyll mode (mode 4), resulting in a pixel size of 17 m and 18 spectral bands in the range 485-802 nm. Band 15, centred at 761 nm, was not used because it sampled an O_2 absorption feature and was noisy. The most backward image did not cover the study area. The acquisition geometry of the 4 images used in the study is shown in Figure 1.

Table 1: Stands characteristics and model inputs.

Stand		YOUNG	OLD1	OLD2
Age (years)		29	100	75
Density (trees/ha)		1450	160	420
DBH (cm)		14	53	37
Canopy	PAI	8.88	5.73	7.35
	fB	0.13	0.23	0.4
	D	0	0	0.1
	Hot	0.01	0.01	0.01
	LIDF	Spherical	Spherical	Spherical
	Cv	0.9	0.55	0.7
	Zeta	0.34	0.24	0.26
Needle	Cab (µg/cm^2)	55	60	65
	Cw (cm)	0.02	0.02	0.02
	Cdm (g/cm^2)	0.04	0.04	0.04
	Cs	0	0	0
	N	2.7	2.5	2.3
Bark	Cab (µg/cm^2)	10		
	Cw (cm)	0		
	Cdm (g/cm^2)	0.5		
	Cs	15		
	N	10		

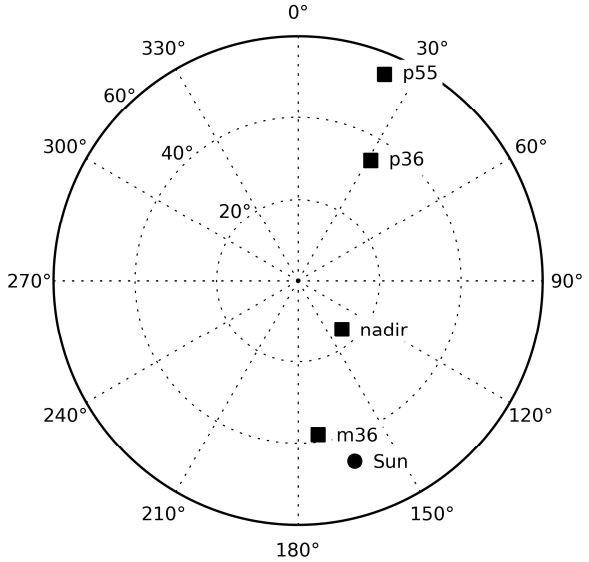

Figure 1. Acquisition geometry of the multi-angular CHRIS/PROBA data.

2.2 Coupled canopy-atmosphere model and parameterization

The SLC model is an integrated soil-leaf-canopy model (Verhoef and Bach, 2007). It uses the 4SAIL2 canopy model, which is the latest version of the SAIL model. 4SAIL2 includes crown clumping thanks to Zeta and Cv, as well as 2 canopy layers which can have different compositions in green and brown elements as defined by fB and the dissociation factor D (for D=0, the elements are homogeneously distributed in the 2 layers, and for D=1, all the green elements are in the top layer). These 2 features make 4SAIL2 appropriate for modelling forests. The leaf inclination distribution function (LIDF) was chosen spherical, as this is the best description of randomly oriented spruce needles. The PROSPECT model, modified to include the concentration of senescent material (Cs) (Verhoef and Bach, 2003), was used to simulate needle and bark materials. The specific absorption coefficients and refractive index at 1 nm resolution were taken from Feret et al. (2008). The PROSPECT inputs were optimized to match the measured bark signature, and for each stand, the inputs for the needles were tuned together with the D parameter using the 4 angular TOA radiance measurements. The average background signature was calculated for each stand from the field measurements and input directly into SLC.

The MODTRAN model is a state-of-the-art atmospheric RT model. The atmosphere was assumed constant for the 4 images, the differences in path length due to changing viewing geometry being accounted for by MODTRAN. Urban aerosols were used because of the dominant north wind blowing from an industrial zone and high air concentration of SO_2. The visibility was set to 100 km, which was the smallest value for which the simulated atmospheric path radiance in each observation direction was smaller than all radiances in the corresponding CHRIS image.

The SLC and MODTRAN outputs were resampled to the CHRIS spectral bands using Gaussian approximations of the response functions before implementing the canopy-atmosphere coupling (Laurent et al., 2011). The coupling step calculates the TOA radiance in the observation direction (L_o) by combining the 4 directional reflectance components simulated by SLC with 7 parameters which account for the double pass of the radiation in the atmosphere. The 7 atmospheric parameters are calculated from the outputs of three MODTRAN runs for Lambertian surfaces.

2.3 Local sensitivity analyses

For each observation direction o, the Jacobian matrix $\mathbf{J}_o$ is defined as the matrix of the partial derivatives of the model output L_o with respect to the normalized input parameters p:

$$\mathbf{J}_o = \left\lfloor j_{o,i,k} \right\rfloor_{1\le i\le n_b,\,1\le k\le n_p}, \text{ with } j_{o,i,k} = \frac{\partial L_o(\lambda_i)}{\partial p_k}, \qquad (1)$$

where λ_i is the central wavelength of the ith band, n_b is the number of bands and n_p is the number of parameters. The parameters were normalized assuming a uniform distribution over their potential variation range. Canopy and atmospheric parameters were varied by 1% of their potential variation range, except the canopy hotspot parameter (hot) which was varied by 0.005 because of its very small value. For the multi-angular analyses, the Jacobian matrix $\mathbf{J}$ was calculated over the ensemble Θ of observation directions by vertically stacking the $\mathbf{J}_o$ matrices for o in Θ. For each parameter p_k, the influence indicator α_k was defined as:

$$\alpha_k = \sqrt{\frac{\sum_{o\in\Theta}\sum_{i=1}^{n_b} w_i j_{o,i,k}^2}{\sum_{o\in\Theta}\sum_{i=1}^{n_b} w_i}}, \qquad (2)$$

where the *w* terms are weights that account for the irregular spectral distance between the CHRIS bands. To allow easier comparison between stands, the α values were normalized (α_{norm}). Only the most influential parameters having high α_{norm} values can be estimated.

The dimensionality of the estimation problem is the maximum number of variables that can theoretically be estimated. It was assessed by performing a singular value decomposition (SVD) of the **J** matrix (Laurent et al., 2011). The dimensionality was taken as the number of singular values needed to reach 95% of the sum of all singular values.

2.4 Variable estimation

One look-up table (LUT) was built for each stand, making use of the results of the local sensitivity analyses: the number of free variables n_v was chosen as the dimensionality plus one, in order to have one adjustment variable, and the most influential parameters were used as free variables. Each variable was sampled using regular steps, between boundary values chosen using prior knowledge. The non-free parameters were kept at the values in Table 1. For each combination of variable values, the LUT stores the L_o simulation in each observation direction. The cost function χ was defined using the same structure as the α indicator:

$$\chi(v) = \sqrt{\frac{\sum_{o\in\Theta}\sum_{i=1}^{n_b} w_i \left(L_o(\lambda_i, v) - L_{o,ref}(\lambda_i, v)\right)^2}{\sum_{o\in\Theta}\sum_{i=1}^{n_b} w_i}}, \quad (3)$$

where $L_{o,ref}$ is the measured CHRIS radiance in the observing direction *o*, and *v* is the set of variable values considered. After removing the insensitive sets of variables from the LUT (e.g., sets with varying Zeta when Cv = 1), the variable estimation was performed for all the possible combinations of the 4 CHRIS angles. The solution space was defined as the ensemble satisfying $\chi(v) \le \chi_{thresh}$, with $\chi_{thresh} = \chi_{min}$. For each variable, the median of the values in the solution space was taken as the estimate, and the standard deviation as the estimation uncertainty. The quality indicator δ was defined as the average absolute difference between the set of reference values v_{ref} (from Table 1) and the set of estimates v_{est}:

$$\delta = \frac{1}{n_v}\sum_{i=1}^{n_b} \left| v_{est,i} - v_{ref,i} \right| . \quad (4)$$

3. RESULTS AND DISCUSSION

3.1 Simulations

For the YOUNG stand, the simulations matched the CHRIS data well, with a χ value of 2.9 mW/(m^2 sr nm) for Θ = {m36, nadir, p36, p55}, as can also be seen from the spectral and angular simulated signatures presented in Figure 2. The spectral signatures were underestimated in the m36 direction, and overestimated in the nadir, p36 and p55 directions. The fit of the angular signatures was better in the visible than in the NIR. Similar results were observed for the other stands, but with slightly higher χ values: 4.8 mW/(m^2 sr nm) for the OLD1 stand, and 3.9 mW/(m^2 sr nm) for the OLD2 stand for Θ = {m36, nadir, p36, p55}.

The visibility had to be chosen very high so that the simulated atmospheric path radiance (L_{atm}) would be smaller than all radiances in the CHRIS images. L_{atm} constitutes the major part of the radiance in the visible, and a small part in the NIR, so that small errors in the canopy reflectance were less important in the visible than in the NIR, explaining the smaller χ values of the angular signatures in the visible than in the NIR. Despite its turbid medium assumption, SLC was able to produce adequate multi-angular simulations of the 3 spruce stands, thanks to its crown clumping feature. The canopy-atmosphere coupling implemented here, which allows making full use of the 4 directional reflectance components, also participated to the good quality of simulation of the TOA radiance.

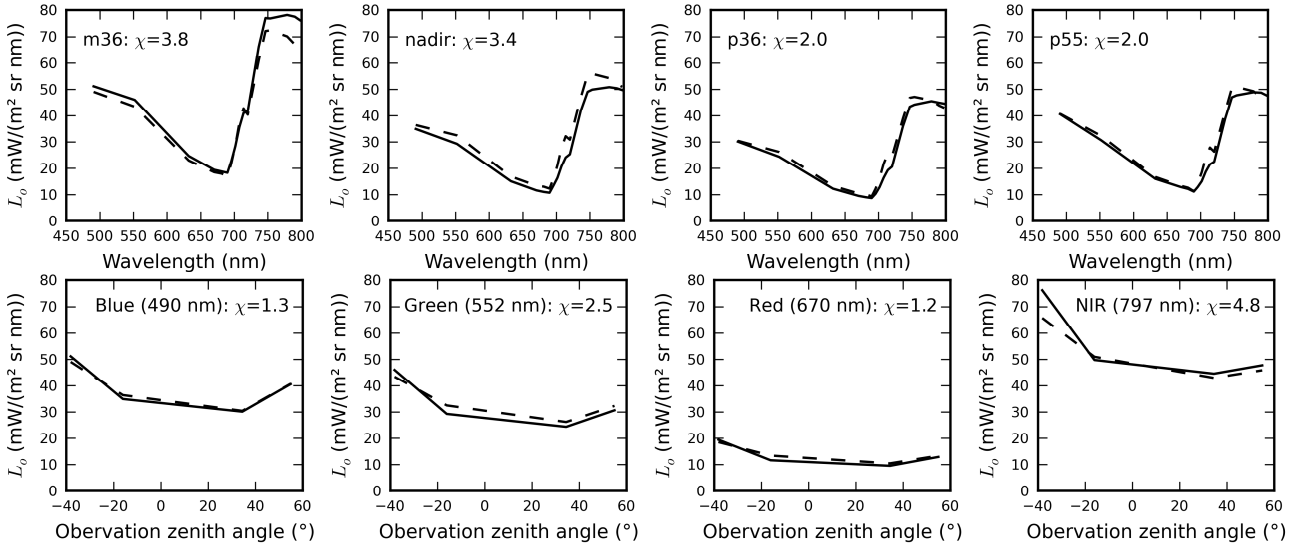

Figure 2. Spectral (top line) and angular (bottom line) TOA radiance simulation results for the YOUNG stand. The plain lines represent the CHRIS measurements, and the dashed lines, the simulations.

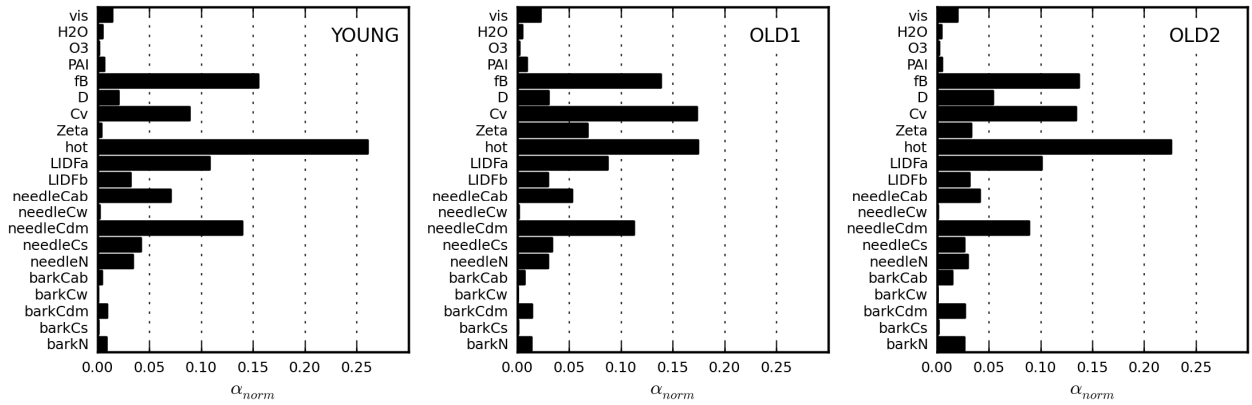

Figure 3. Parameter influences (α_{norm}) for the three stands for Θ = {m36, nadir, p36, p55}.

3.2 Local sensitivity analyses

The 3 stands presented similar profiles of parameter influences for Θ = {m36, nadir, p36, p55} (Figure 3). The atmospheric parameters had very small influence, meaning that they were not going to hamper the variable estimation. This might be limited to a very clear atmosphere. Overall, the canopy and needle parameters were more influential than the bark parameters. These trends were similar for all angular combinations for the 3 stands, despite different angular responses of some structural parameters such as LIDFa and b and hot. Overall, the most influential parameters were: hot, fB, Cv, LIDFa and b, needleCab, needleCdm, D, Zeta, and needleCs. The importance of hot is due to the high PAI of the 3 stands, which causes a wide hotspot effect. The PAI was not influential because of its very high value. As the PAI consists mostly of leaves, it saturates the radiance in the same way as LAI.

For the 3 stands, the dimensionality increased from 3 to 6 when increasing the number of angles from 1 to 4 (Table 2), thus clearly demonstrating the higher potential of multi-angular data over mono-angular data. A dimensionality of 3 is commonly observed for hyperspectral mono-angular data because of data redundancy in contiguous spectral bands. Similarly, each additional angle does not increase the dimensionality by 3, revealing redundancy in the angular data. This was also found by Simic and Chen (2008).

Table 2. Dimensionality based on the singular value decomposition for all possible angular combinations.

Θ	YOUNG	OLD1	OLD2
{nadir}	3	3	3
{m36}	3	3	3
{p36}	3	3	3
{p55}	4	4	4
{nadir, m36}	4	4	4
{nadir, p36}	4	5	5
{nadir, p55}	5	5	5
{m36, p36}	4	4	4
{m36, p55}	4	5	5
{p36, p55}	5	5	5
{nadir, m36, p36}	5	5	5
{nadir, m36, p55}	5	6	6
{nadir, p36, p55}	5	6	6
{m36, p36, p55}	5	6	6
{nadir, m36, p36, p55}	5	6	6

3.3 Variable estimation

Based on the local sensitivity analyses, for each stand, a LUT was built with 7 free variables, following the sampling scheme presented in Table 3. The LIDFa and b and hot parameters were not selected as free variables because a spherical LIDF is the best description of the randomly oriented spruce needles, and the value of 0.01 for hot is common for forests. The value of $\chi_{thresh} = 1.05\chi_{min}$ used to define the solution space was chosen by trial and error, based on the recommendation of Weiss et al. (2000) that the solution space should not exceed 0.5% of the total number of entries in the LUT.

Table 3. Variable sampling scheme used for building the LUTs.

Parameter	Min	Max	Step	# values
fB	0	0.6	0.1	7
Cv	0.4	1	0.1	7
D	0	1	0.2	6
Zeta	0.2	0.4	0.04	6
NeedleCab (µg/cm^2)	40	80	10	5
NeedleCdm (g/cm^2)	0.01	0.07	0.01	7
NeedleCs	0	0.03	0.01	4

For the YOUNG stand, the best radiance match was obtained for Θ = {nadir, p36, p55} (χ_{thresh} = 0.656), and the best estimates for Θ = {nadir, p36, p55}, and Θ = {m36, p36, p55} (δ = 0.426) (Table 4). Similarly, in the other stands, the best radiance match and the best estimates were obtained for different angular combinations: in the OLD1 stand, the best radiance match was obtained for Θ = {nadir} (χ_{thresh} = 0.926), and the best estimates for Θ = {m36, p55} and Θ = {nadir, m36, p55} (δ = 0.396); and in the OLD2 stand, the best radiance match was obtained for Θ = {nadir, p36, p55} (χ_{thresh} = 1.223), and the best estimates for Θ = {nadir, p55} (δ = 0.292).

Considering the dimensionality results, it was expected that the more angles used in Θ, the better the estimates would be. The results, however, showed that the best estimates were not obtained with Θ = {m36, nadir, p36, p55}, but with combinations using 2 to 3 angles, although the successful combinations always had both backward and forward angles (the nadir image was actually acquired in the backward direction, see Figure 1). In addition, the combinations that gave the best radiance match did not give the best estimates, except for the YOUNG stand. This finding supports Gascon et al. (2007) who pointed out the difficulty of fully exploiting the information contained in multi-angular data. To improve the estimation performance, one might introduce angular

Table 4. Estimation results for the YOUNG stand for all possible angular combinations. The values in brackets represent the estimation uncertainty.

Θ	Cv	fB	needleCab (µg/cm^2)	needleCdm (g/cm^2)	D	Zeta	needleCs	δ	χ_{thresh}
{m36}	0.9 (0.04)	0.4 (0.09)	50.0 (0.00)	0.01 (0.00)	0.4 (0.18)	0.28 (0.07)	0.02 (0.01)	0.544	1.699
{nadir}	0.8 (0.04)	0.2 (0.14)	70.0 (5.00)	0.05 (0.01)	1.0 (0.31)	0.28 (0.07)	0.02 (0.01)	0.742	1.088
{p36}	0.8 (0.08)	0.3 (0.19)	70.0 (4.01)	0.04 (0.01)	0.6 (0.25)	0.28 (0.07)	0.02 (0.01)	0.544	0.981
{p55}	0.8 (0.09)	0.4 (0.14)	70.0 (0.00)	0.02 (0.01)	0.4 (0.22)	0.28 (0.07)	0.02 (0.01)	0.594	1.018
{nadir, m36}	0.6 (0.03)	0.3 (0.20)	50.0 (3.81)	0.02 (0.00)	0.8 (0.24)	0.32 (0.05)	0.02 (0.01)	0.772	1.756
{nadir, p36}	0.7 (0.05)	0.2 (0.13)	70.0 (3.87)	0.04 (0.00)	0.6 (0.30)	0.24 (0.06)	0.01 (0.01)	0.559	0.752
{nadir, p55}	0.8 (0.00)	0.2 (0.17)	80.0 (4.50)	0.05 (0.01)	0.8 (0.45)	0.32 (0.06)	0.02 (0.01)	0.673	0.793
{m36, p36}	0.7 (0.03)	0.3 (0.18)	50.0 (3.51)	0.02 (0.01)	0.6 (0.23)	0.4 (0.02)	0.02 (0.01)	0.643	1.686
{m36, p55}	1.0 (0.00)	0.3 (0.16)	50.0 (4.96)	0.03 (0.01)	0.4 (0.25)	Non-influent	0.02 (0.01)	0.485	1.891
{p36, p55}	0.9 (0.02)	0.3 (0.16)	80.0 (4.50)	0.035 (0.01)	0.4 (0.27)	0.3 (0.07)	0.02 (0.01)	0.460	0.747
{nadir, m36, p36}	0.7 (0.05)	0.2 (0.18)	60.0 (0.00)	0.02 (0.01)	0.6 (0.24)	0.4 (0.02)	0.01 (0.01)	0.589	1.379
{nadir, m36, p55}	0.8 (0.05)	0.3 (0.16)	60.0 (1.41)	0.03 (0.01)	0.6 (0.29)	0.4 (0.03)	0.01 (0.01)	0.539	1.673
{nadir, p36, p55}	0.8 (0.00)	0.1 (0.13)	80.0 (5.00)	0.04 (0.01)	0.4 (0.39)	0.28 (0.07)	0.02 (0.01)	0.426	0.656
{m36, p36, p55}	0.9 (0.06)	0.4 (0.16)	60.0 (3.35)	0.03 (0.01)	0.4 (0.25)	0.36 (0.05)	0.02 (0.01)	0.426	1.537
{nadir, m36, p36, p55}	0.8 (0.05)	0.3 (0.16)	60.0 (0.67)	0.03 (0.01)	0.4 (0.30)	0.4 (0.03)	0.01 (0.01)	0.440	1.302

weights to account for poorer simulation accuracy at very oblique angles, or include the measurement error in the inversion process. However, compensation effects between angles in the cost function might also be a cause of the poor estimation performance. For example a set of variable values having very good radiance match in the forward direction and poor in the backward direction can have a smaller χ value than a better set of variable values having similar radiance match in all directions. In addition, the quality of the reference data for the variables was also problematic in some cases, for example for Cv which was estimated by classifying an AISA image as no in-situ measurement was available.

Finally, in this study, the pixels belonging to each stand were selected manually in each image, thus avoiding co-registration issues. When processing entire images, the quality of the co-registration would be critical to any multi-angular study.

4. CONCLUSION

This paper presented the first case study of estimating forest variables directly from multi-angular TOA radiance data by inverting a physically-based RT canopy-atmosphere model. The results showed that the dimensionality of the estimation problem increased from 3 to 6 when increasing the number of angles from 1 to 4, thus demonstrating the higher potential of multi-angular data for estimating forest variables. The estimation results, however, did not match with the expectation that using all 4 angles together would yield the best estimates, thus pointing out the difficulty of making full use of the additional information contained in the multi-angular data.

The coupled SLC-MODTRAN model provided good simulations of the forest TOA radiances measured by CHRIS. The canopy-atmosphere coupling implemented in this study allowed making full use of the 4 directional reflectance components provided by SLC and thus benefited the simulation accuracy and subsequently the estimation performance.

5. ACKNOWLEDGEMENT

The data collection was conducted under ESA/PECS project No. 98029 and provided by the Institute of Systems Biology and Ecology, Academy of Sciences of the Czech Republic. The authors wish to thank Petr Lukeš and Lucie Homolová for their help with the data and Allard de Wit for his assistance with model implementation and LUTs.

6. REFERENCES

Feret, J.B., François, C., Asner, G.P., Gitelson, A.A., Martin, R.E., Bidel, L.P.R., Ustin, S.L., Le Maire, G., & Jacquemoud, S., 2008. PROSPECT-4 and 5: Advances in the leaf optical properties model separating photosynthetic pigments. *Remote Sensing of Environment, 112*(6), pp. 3030-3043.

Gascon, F., Gastellu-Etchegorry, J.P., & Leroy, M., 2007. Using multi-directional high-resolution imagery from POLDER sensor to retrieve leaf area index. *International Journal of Remote Sensing, 28*(1), pp. 167-181.

Heiskanen, J., 2006. Tree cover and height estimation in the Fennoscandian tundra-taiga transition zone using multiangular MISR data. *Remote Sensing of Environment, 103*(1), pp. 97-114.

Homolová, L., Malenovský, Z., Hanuš, J., Tomášková, I., Dvořáková, M., & Pokorný, R., 2007. Comparison of different ground techniques to map leaf area index of Norway spruce forest canopy. In M.E. Schaepman, S. Liang, N.E. Groot & M. Kneubühler (Eds.), *10th ISPMSRS*. Davos, Switzerland: Intl. Archives of the Photogrammetry, Remote Sensing and Spatial Information Sciences.

Huber, S., Koetz, B., Psomas, A., Kneubühler, M., Schopfer, J., Itten, K., & Zimmermann, N.E., 2010. Impact of multiangular information on empirical models to estimate canopy nitrogen concentration in mixed forest. *Journal of Applied Remote Sensing, 4*(043530), pp.

Laurent, V.C.E., Verhoef, W., Clevers, J.G.P.W., & Schaepman, M.E., 2011. Estimating forest variables from top-of-atmosphere radiance satellite measurements using coupled radiative transfer models. *Remote Sensing of Environment, 115*(4), pp. 1043-1052.

Lukeš, P., 2009. Retrieval of canopy cover of the Norway spruce stands in the Bily Kriz area (CZ) from classification of AISA Eagle data. In

Pandya, M.R., Singh, R.P., & Panigrahy, S., 2007. Directional reflectance of vegetation targets: Simulation of its space measurements by coupling atmospheric and biophysical radiative transfer models. *Indian Journal of Radio & Space Physics, 36*(3), pp. 219-228.

Rautiainen, M., Lang, M., Mõttus, M., Kuusk, A., Nilson, T., Kuusk, J., & Lükk, T., 2008. Multi-angular reflectance properties of a hemiboreal forest: An analysis using CHRIS PROBA data. *Remote Sensing of Environment, 112*(5), pp. 2627-2642.

Schaepman, M.E., Ustin, S.L., Plaza, A.J., Painter, T.H., Verrelst, J., & Liang, S., 2009. Earth system science related imaging spectroscopy-An assessment. *Remote Sensing of Environment, 113*(SUPPL. 1), pp. S123–S137.

Simic, A., & Chen, J.M., 2008. Refining a hyperspectral and multiangle measurement concept for vegetation structure assessment. *Canadian Journal of Remote Sensing, 34*(3), pp. 174-191.

Verhoef, W., & Bach, H., 2003. Simulation of hyperspectral and directional radiance images using coupled biophysical and atmospheric radiative transfer models. *Remote Sensing of Environment, 87*(1), pp. 23-41.

Verhoef, W., & Bach, H., 2007. Coupled soil-leaf-canopy and atmosphere radiative transfer modeling to simulate hyperspectral multi-angular surface reflectance and TOA radiance data. *Remote Sensing of Environment, 109*(2), pp. 166-182.

Weiss, M., Baret, F., Myneni, R.B., Pragnère, A., & Knyazikhin, Y., 2000. Investigation of a model inversion technique to estimate canopy biophysical variables from spectral and directional reflectance data. *Agronomie, 20*(1), pp. 3-22.